Human Molecular Genetics, 2004, Vol. 13, No. 11 ***1117–1129***
DOI: 10.1093/hmg/ddh130
Advance Access published on April 21, 2004

Laforin preferentially binds the neurotoxic starch-like polyglucosans, which form in its absence in progressive myoclonus epilepsy

Elayne M. Chan[1], Cameron A. Ackerley[2], Hannes Lohi[1], Leonarda Ianzano[1], Miguel A. Cortez[3], Patrick Shannon[4], Stephen W. Scherer[1] and Berge A. Minassian[1,3,*]

[1]Program in Genetics and Genomic Biology, Research Institute, The Hospital for Sick Children and Department of Molecular and Medical Genetics, the University of Toronto, Toronto, M5G 1X8, Canada, [2]Division of Pathology, Department of Pediatric Laboratory Medicine and [3]Division of Neurology, Department of Pediatrics, The Hospital for Sick Children, Toronto, M5G 1X8, Canada and [4]Department of Neuropathology, Toronto Western Hospital and the University of Toronto, Toronto, M5T 2S8, Canada

Received January 23, 2004; Revised and Accepted April 2, 2004

Lafora disease (LD) is a fatal and the most common form of adolescent-onset progressive epilepsy. Fulminant endoplasmic reticulum (ER)-associated depositions of starch-like long-stranded, poorly branched glycogen molecules [known as polyglucosans, which accumulate to form Lafora bodies (LBs)] are seen in neuronal perikarya and dendrites, liver, skeletal muscle and heart. The disease is caused by loss of function of the laforin dual-specificity phosphatase or the malin E3 ubiquitin ligase. Towards understanding the pathogenesis of polyglucosans in LD, we generated a transgenic mouse overexpressing inactivated laforin to trap normal laforin's unknown substrate. The trap was successful and LBs formed in liver, muscle, neuronal perikarya and dendrites. Using immunogold electron microscopy, we show that laforin is found in close proximity to the ER surrounding the polyglucosan accumulations. In neurons, it compartmentalizes to perikaryon and dendrites and not to axons. Importantly, it binds polyglucosans, establishing for the first time a direct association between the disease-defining storage product and disease protein. It preferentially binds polyglucosans over glycogen *in vivo* and starch over glycogen *in vitro*, suggesting that laforin's role begins after the appearance of polyglucosans and that the laforin pathway is involved in monitoring for and then preventing the formation of polyglucosans. In addition, we show that the laforin interacting protein, EPM2AIP1, also localizes on the polyglucosan masses, and we confirm laforin's intense binding to LBs in human LD biopsy material.

INTRODUCTION

Lafora disease (LD) is an autosomal recessive progressive myoclonus epilepsy characterized by generalized tonic–clonic and myoclonic seizures, progressive neurological deterioration and death within 10 years of onset. The disease manifests in early adolescence and is associated with conspicuous inclusions, Lafora bodies (LBs), in several tissues including brain, liver, skeletal muscle and heart (1,2). LBs are composed of dense aggregates of fibrils shown to be glucose polymers, termed polyglucosans (3). Polyglucosans are more similar to starch than to glycogen: they have long strands and lack the symmetric branching pattern of glycogen needed to allow suspension in the cytoplasm (4–6). Formation of LBs appears to initiate in association with the endoplasmic reticulum (ER) (7,8). In brain, LBs form exclusively in neuronal perikarya and dendrites and not in axons, and they are not present in neuroglia (5).

LD is caused by mutations in the *EPM2A* gene (9) encoding a dual-specificity phosphatase (DSP) (laforin) (10,11), or in the recently identified *EPM2B* gene encoding a putative E3 ubiquitin ligase (malin) (12). An *Epm2a* knockout mouse (13) and a naturally occurring *Epm2b* deficient dog (E.J. Young *et al.*, manuscript in preparation) have been characterized, each closely replicating the human condition.

The subcellular locations of laforin and malin have been studied in epitope-tagged tissue culture experiments. Malin was shown to localize at the ER and nucleus (12), and

*To whom correspondence should be addressed. Tel: +1 4168136291; Fax: +1 4168136334; Email: bminass@sickkids.ca

laforin on ER-associated ribosomes (10,11) and, through its carbohydrate-binding domain, on glycogen (14,15). To date, localization experiments in whole tissues have not been possible, owing to the unavailability of antibodies that are able to recognize either native protein.

In the present work, we describe an *EPM2A* transgenic mouse model of LD, which provides key new cellular localization information about laforin and its role in progressive myoclonus epilepsy. Laforin expressed from the transgene in these mice contains an amino acid transversion, which results in a dominant-negative effect and LD pathology. It is also tagged with the myc epitope allowing us to determine its precise location in brain, namely, in neuronal perikarya and dendrites. In all tissues examined, laforin is shown to bind LBs, and in liver, where LBs consist of a mixture of polyglucosans and normal glycogen [as in the human disease (16–18)], to preferentially associate with polyglucosans. Our collective results suggest a role for the laforin pathway in the quality control of glycogen formation.

RESULTS

Generation of mice expressing a dominant-negative myc–laforin transgene

Inactivation of the catalytic cysteine residue of DSP and protein tyrosine phosphatase (PTP) enzymes results in tight binding and trapping of substrate. Transgenic introduction of DSP and PTP mutated in this fashion has been used extensively to generate animal models with functional deficiency of the corresponding native proteins (19–21). Here, we used the pCAGGS expression vector (22) to deliver human *EPM2A* containing a DSP-inactivating point mutation (797G > C, C266S) that is tagged with the myc epitope (11) (Fig. 1A). The transgene was successfully integrated into 10 founder lines as identified by both PCR and Southern analysis (Fig. 1B and C).

To examine the relative expression levels between the endogenous wild-type *EPM2A* transcript and the mutant *EPM2A* transgene, quantitative real-time RT–PCR was performed. Brain samples from the transgenic line were analyzed and results indicated a 100-fold overexpression of the transgene (β-actin promoter) over the endogenous wild-type counterpart (Fig. 1D).

Of 10 founder lines with integrated transgene, one expressed myc–laforin in brain, skeletal muscle, heart and liver (Fig. 1E). A second line expressed in brain, heart and liver only. Two mice from the first line, and two wild-type littermates, were studied by electrocorticography and pathological analysis at each of 8, 12 and 20 months of age. Two transgenic and two wild-type mice from the second line were studied at 12 months. Results in both lines were similar. None of the mice exhibited clinical or electrographic seizures, or neurodegeneration. All the transgenics exhibited LB formation. We describe the subcellular localizations of myc–laforin and LBs, and their relationship.

Brain: myc–laforin distributes to neuronal somas and dendrites, but not to axons

With light microscopy, diffuse staining of neuronal cell bodies with the myc antibody was present in transgenics but not in controls. All neuronal types from all brain regions were stained (Fig. 2A–C) but neuroglia were not. Particularly, strikingly outlined were cerebellar Purkinje cell somas and dendrites (Fig. 2A) and stellate neurons (Fig. 2B and C). Other strongly reactive neuronal populations include pyramidal cells and dendrites of the cornu ammonis, the somas and neuropil within the granular cell layer of the fascia dentata, the neuropil of the thalamus, the tectum, the striatum, some neurons of the cerebellar deep nuclei and multiple brainstem nuclei. Within the cerebral cortex, both large and small cortical neurons showed immunoreactivity that was not restricted to any particular cortical layer. Subcortical fibers, including axons of cerebellar Purkinje cells (Fig. 2D), did not stain. Choroid plexus stained positive in mutant and wild-type animals, indicating an endogenous target for the myc antibody in this location.

With myc immunogold electron microscopy, the most striking finding was the distribution of gold particles at synapses. Invariably, the particles were on the post-synaptic side of the cleft within the dendrite cytoplasm and not in the presynaptic bouton (Fig. 2E). In neuronal somas, the signal was always near ER, but not on ribosomes (Fig. 2F). No signal was detected in myelinated fibers. Unmyelinated fibers containing ribosomes (i.e. dendrites) frequently had signal, but again the gold particles were found in the cytoplasm and not in association with the ribosomes (Fig. 2E).

Brain: LB formation and localization of myc–laforin on LBs

Compaction of polyglucosans in LBs prevents their digestion by amylase. Amylase (diastase)-resistant periodic acid-Schiff staining (PASD) is the histochemical marker of LBs (2). Examination of brains from transgenic mice with PASD revealed extensive LB formation in the hippocampus, with lesser amounts in the basal forebrain and sparse distribution throughout the rest of the brain. The low frequency of LBs outside the hippocampus in these animals is a major difference with the human disease. Twelve-month-old animals had more LBs than the younger mice in all regions, but no further significant increase was noted at 20 months. In wild-type mice, extremely faint hippocampal neuropil staining could be seen in the oldest animals, and no LB was present outside the hippocampus.

LBs were in the neuropil (Fig. 3A and C) and within neuronal cell bodies (Fig. 3E), but not in axonal tracts. They were found readily with electron microscopy in these same locations (Fig. 4A–E), and were not present in any glia. They were mostly spherical in shape with a dense accumulation of fibrillar material in the center. In the soma, they occupied a position near the perinuclear ER. In the neuropil, they were present within dendrites (Fig. 4A–E).

On immunohistochemical analysis with the myc antibody, concentrated staining was present on the LBs (Fig. 3B and D). In addition, diffusely throughout the molecular layer of the cortex and in some hippocampal and cerebral neurons, punctate structures became evident, likely representing smaller LBs. With immunogold electron microscopy, a high density of gold particles intensely labeled small and large LBs (Fig. 4D and E), demonstrating an important localization of myc–laforin on LBs.

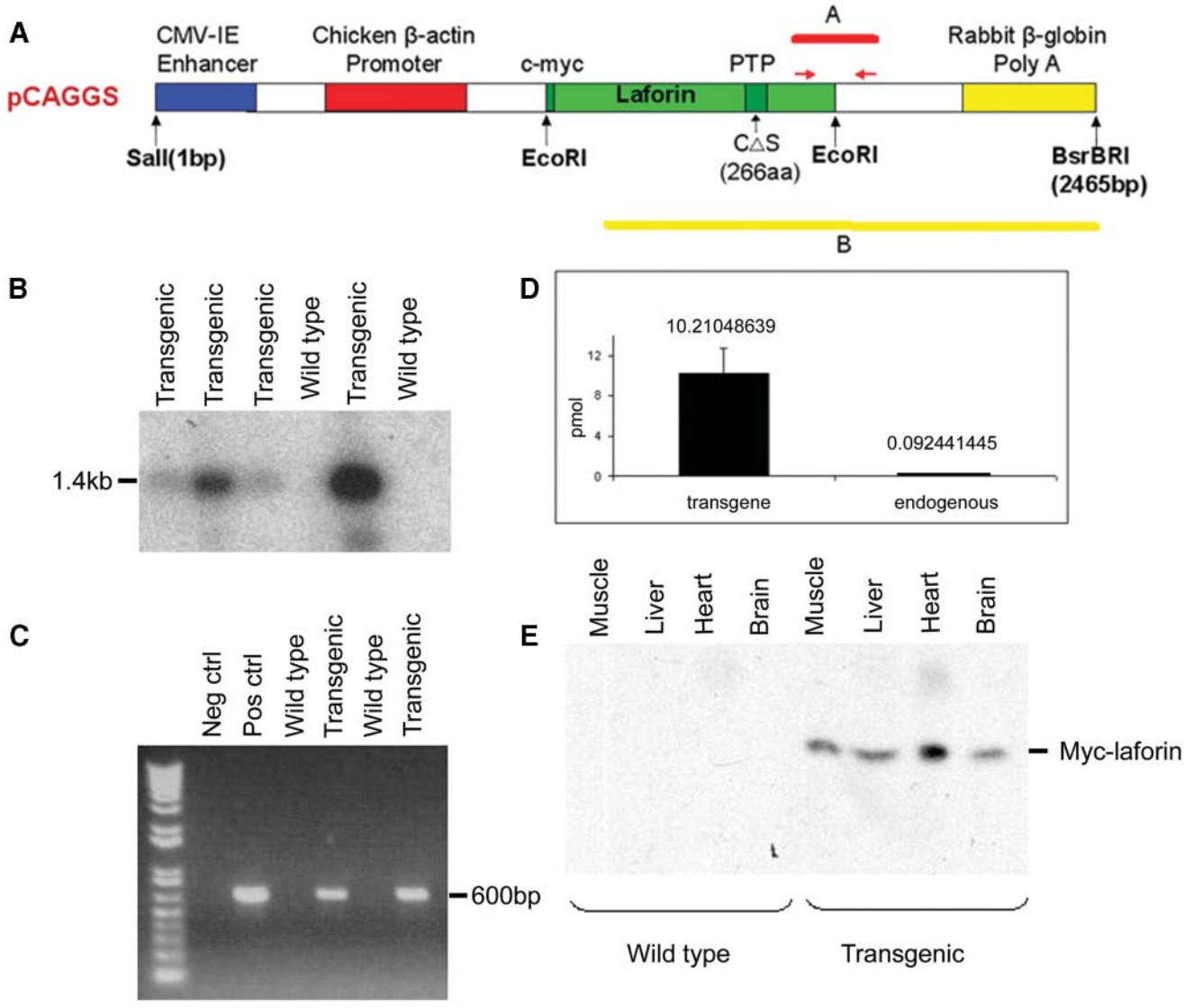

Figure 1. Generation of myc–laforin CΔS transgenic mice. (**A**) The transgene was driven by a chicken β-actin promoter in the pCAGGS expression vector. The transgene encoded for a myc-tagged laforin fusion protein carrying a cysteine to serine mutation at amino acid 266 in the active site of the PTP domain. The transgene was excised from the plasmid using the restriction enzymes *Sal* I and *Bsr* BRI generating a 2465 bp fragment that was used in generating transgenic mice. (**B**) Southern blot analysis using probe B shown in (A) identifies a 1.4 kb band in transgenic and not wild-type mice. (**C**) PCR of transgene-specific sequence [fragment A shown in (A)] generates a 600 bp fragment in transgenic and not in wild-type mice. (**D**) Expression levels of transgenic and endogenous *EPM2A* in transgenic mouse brain. (**E**) Western blot analysis identifies myc–laforin expression in muscle, liver, heart and brain in a single founder line and not in wild-type littermates.

Skeletal and cardiac muscles: myc–laforin on LBs and post-synaptic compartment

A high proportion of skeletal muscle fibers in transgenic animals contained large polyglucosan pools. These were present primarily in the subsarcolemma (Fig. 5A) adjacent to myonuclei and at the neuromuscular junctions (NMJs) (Fig. 5B and C). Some were also present in the sarcoplasm between the sarcomeres (data not shown). Similar accumulations were observed in the myocardium (Fig. 5D).

The myc antibody strongly stained the polyglucosan fibrils (Fig. 5A). Signal was also found in association with components of the sarcotubular network (data not shown) and at the NMJ. In the latter, the gold signal was found exclusively on the secondary synaptic clefts and in the junctional sarcoplasm (i.e. post-synaptic side), but not in the nerve terminus (pre-synaptic side) (Fig. 5E).

Liver: myc–laforin binds polyglucosans preferentially over glycogen

Light microscopic and ultrastructural examinations demonstrated numerous LBs in hepatocytes, occupying the majority of the cytoplasm and displacing the nucleus and other

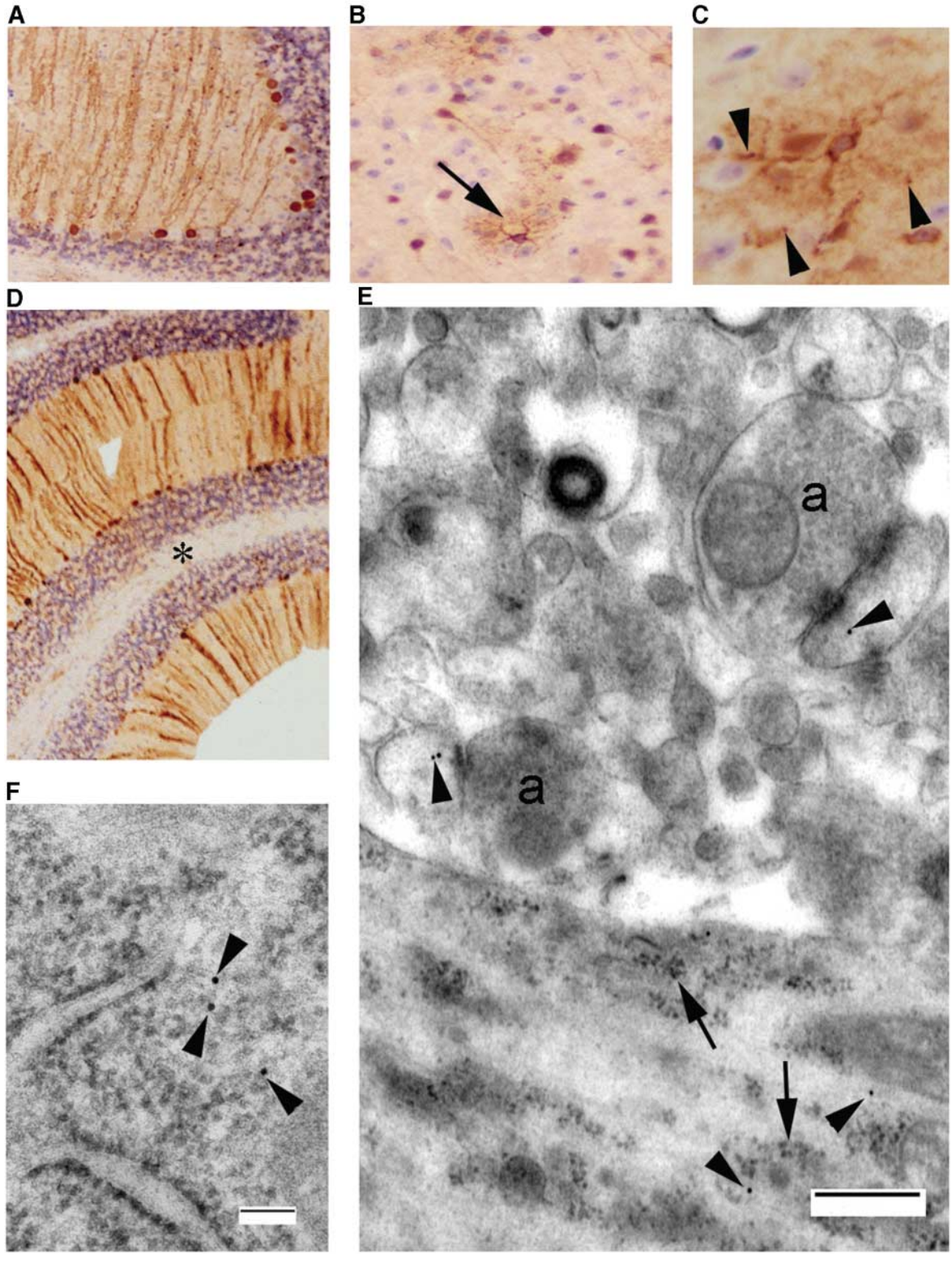

Figure 2. This and all subsequent mouse pathology figures are from 12-month-old mice. (**A**) Cerebellum stained for myc from an affected animal. Note the intense staining of the Purkinje cells. Picture width is 1.5 mm. (**B**) Stellate (arrow) and pyramidal neurons from the cortex stained for myc. Picture width is 0.75 mm. (**C**) High power of a stellate neuron stained for myc. Note the punctate structures (arrowheads) in the extremities of the cell. Picture width is 0.5 mm. (**D**) Cerebellum stained for myc. Note the absence of any stain in the white matter (asterisk). Picture width is 2 mm. (**E**) Immunogold labeled cortex from an affected animal. Gold label was seen only in the post-synaptic regions (arrowheads) and not in the axons (a). Gold label was also seen in the cytoplasm of the dendrites (arrowheads) but not associated with ribosomes (arrows). Bar equals 0.5 μm. (**F**) Immunogold labeling (arrowheads) in close proximity to the rough ER but not associated with ribosomes. Bar equals 0.1 μm.

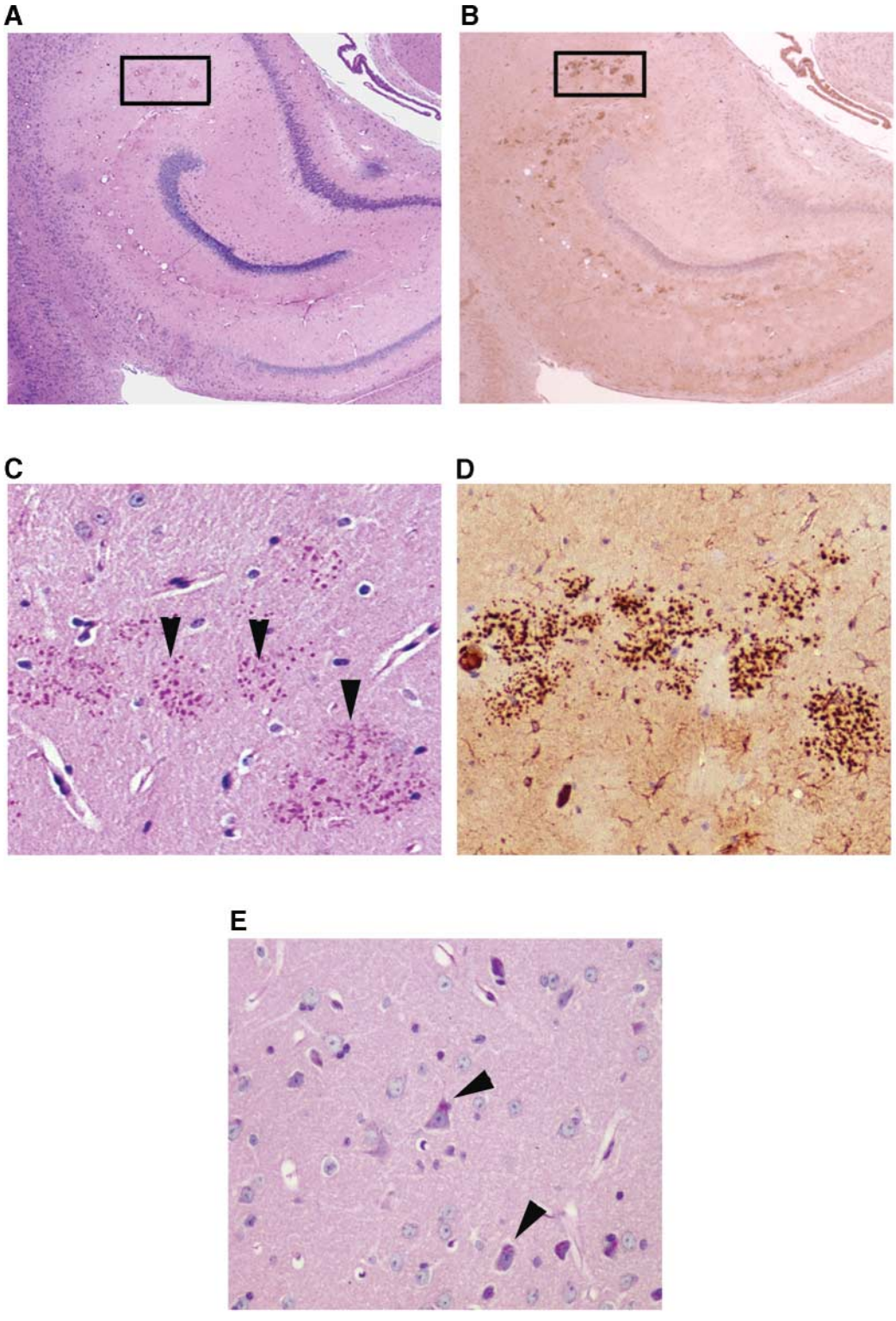

Figure 3. (**A**) Low power of brain from an affected mouse including hippocampus that has been PASD stained. Note the PASD positive material within the box. (**B**) Identical field as (A) from a deeper section of the same block that has been immunoperoxidase stained for myc. Note the foci of myc stained neurons throughout the field that correlate with the PASD stained section. With higher magnification (Fig. 2C), these neurons exhibit punctate densely stained dendritic structures, which are likely small LBs seen with the electron microscope (Fig. 4). Picture width is 5 mm. (**C**) Higher power of boxed region in (A). PASD staining of hippocampus from an affected mouse. Note the numerous LBs in clusters in the neuropil (arrowheads). Picture width is 1 mm. (**D**) Higher power of boxed region in (B) and identical field to panel (C) several sections deeper in the block, which has been immunoperoxidase stained against myc. Note the intensely stained punctate structures identical in size and shape to the PASD stained material in (C). Picture width is 1 mm. (**E**) As in (C), showing PASD stained LBs in the neuronal cell body cytoplasm (arrowheads). Picture width is 1 mm.

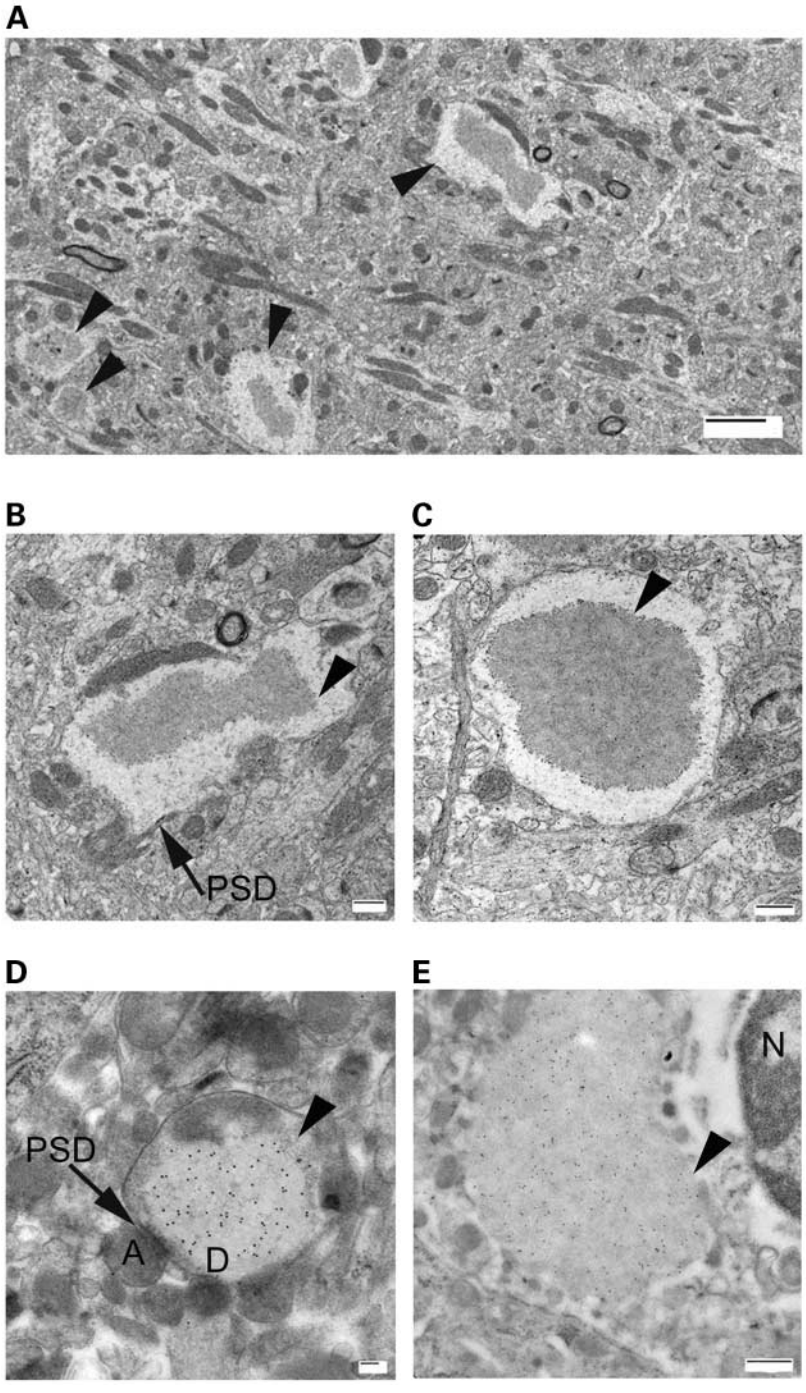

Figure 4. (**A**) Low power electron micrograph of neuropil from an affected animal. Several LBs (arrowheads) are present. Bar equals 2 μm. (**B**) Higher power of one of the LBs present in (A). Note the post-synaptic density (PSD, arrow) and the condensed fibrillar center of the LB (arrowhead). Bar equals 0.5 μm. (**C**) Another example of an LB (arrowhead). Bar equals 0.5 μm. (**D**) myc immunogold labeled LB (arrowhead) from the neuropil of an affected animal. Note the axon (A), dendrite (D) and post-synaptic density (PSD, arrow). Bar equals 0.1 μm. (**E**) Immunogold labeled perikaryal LB (arrowhead). Note the adjacent nucleus (N). Bar equals 0.5 μm.

organelles peripherally (Fig. 6A). They consisted of a mixture of polyglucosan fibrils and more normal appearing glycogen rosettes (Fig. 6B).

With myc staining, the majority of the label was in the storage compartment. Here, the signal was specifically present directly on the polyglucosan fibrils and fibrillar clumps and not on the surrounding normal glycogen (Fig. 6D–F).

Gold signal was also present in a second location: in the vicinity of ER found in the periphery of LBs, but not inside

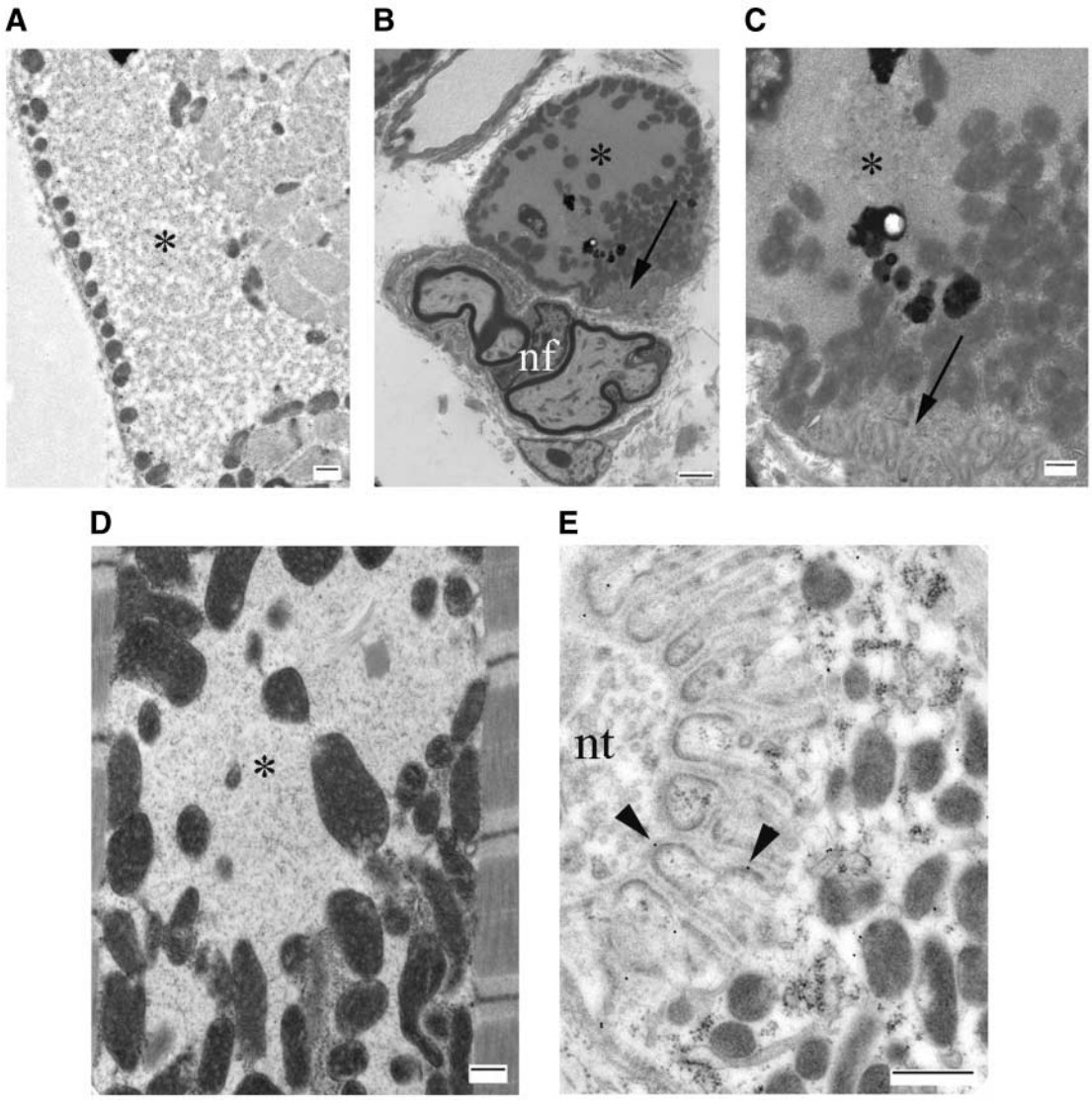

Figure 5. (**A**) Intense myc immunogold labeling of a subsarcolemmal LB from an affected animal (asterisk). Bar equals 0.5 μm. (**B**) Low power electron micrograph of a myofiber that contains an LB (asterisk), an NMJ (arrow) and a nerve fiber (nf). (**C**) Higher power of (B). A large LB (asterisk) is seen in the perinuclear sarcoplasm of an innervated myofiber. The secondary synaptic clefts (arrow) of the NMJ are present in the micrograph. Bar equals 0.5 μm. (**D**) LB in myocardium (asterisk). Note the fibrillar appearance of its contents. Bar equals 0.5 μm. (**E**) myc immunogold labeled NMJ. Note that the label is confined to the secondary synaptic clefts (arrowheads) and sarcoplasm and not to the nerve terminus (nt). Bar equals 0.5 μm.

ER cisterns, and clearly not in direct association with ribosomes. It was impossible to distinguish whether the gold signal near ER is on polyglucosan material, although the electron microscopic appearance is suggestive (Fig. 6E and G; see also Fig. 2F)

Of the other cellular organelles, none stained, except for mitochondria (Fig. 6E). The proportion of stained mitochondria was too small to conclude a definitive association, although this point merits further investigation.

Native human laforin binds LBs in LD

We previously generated a number of antibodies sensitive on western blots to recombinant laforin, but as mentioned earlier we were unable to detect the native protein in normal tissues. Observation of intense LB labeling by myc–laforin in the transgenic mice led us to consider whether native laforin would also cluster on LBs in LD. We stained the brain biopsy of an LD patient carrying *EPM2B* mutations (and no *EPM2A* mutation) with R60, one of our anti-human laforin polyclonal antibodies, and demonstrate intense LB labeling (Fig. 7A and B), indicating concentration of laforin onto the LB polyglucosan masses. This observation shows that laforin's polyglucosan binding is independent of the artificial conditions in the transgenic cells (overexpression, epitope tag, point mutation and possible trapped substrate).

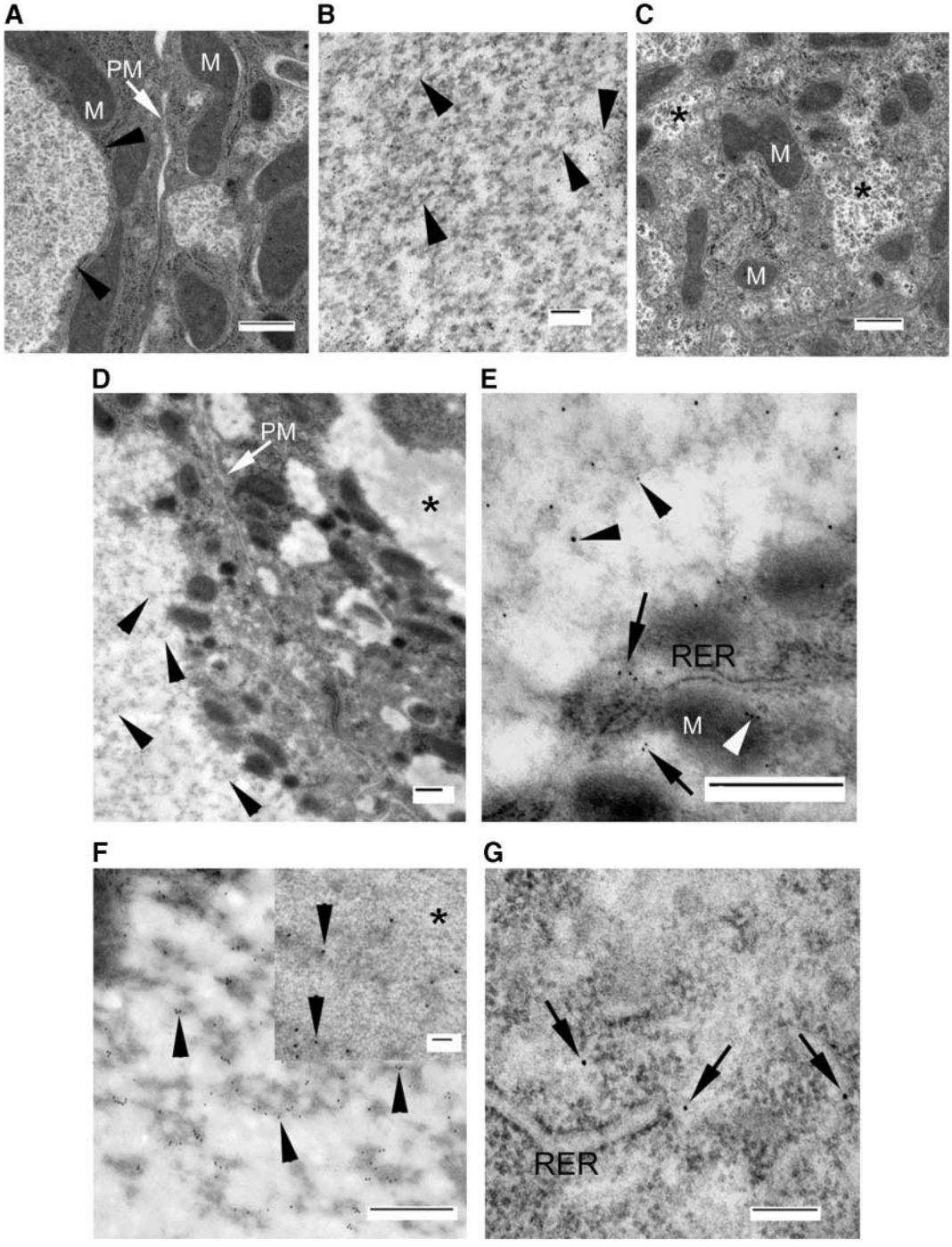

Figure 6. (**A**) Transmission electron micrograph of an affected hepatocyte. Note how the LB (arrowhead) is pressing the cytoplasm to the periphery of the cell. The plasma membrane (PM, white arrow) and mitochondria (M) are present in the micrograph. Bar equals 0.5 μm. (**B**) Higher magnification in another hepatocyte. Fibrillar material (arrowheads) is seen throughout the field of view. Bar equals 0.1 μm. (**C**) Hepatocyte from a wild-type littermate. Note the lakes of normal glycogen rosettes (asterisks). A number of mitochondria (M) are visible in the micrograph. Bar equals 0.5 μm. (**D**) Electron micrograph of a myc immunogold stained liver section. An affected cell on the left side of the image is separated from the adjacent unaffected cell by the plasma membrane (PM, white arrow). Fibrillar storage material (arrowheads) in an affected cell (left side of image); gold is just visible on the fibrillar material at this low magnification. Normal glycogen lake (asterisk) in the adjacent unaffected cell (right side of image) contains no label. Appearance of normal glycogen in sections prepared for immunostaining differs from (C) because osmium cannot be used in these experiments. Bar equals 0.5 μm. (**E**) Higher power of the periphery of an LB. Gold label is seen associated with fibrillar material in the LB (black arrowheads). Label, depicted by arrows was also found in the cytoplasm in close proximity to the rough ER (RER). In this image a mitochondrion (M) is also labeled (white arrowhead). Bar equals 0.5 μm. (**F**) myc staining in an LB. Gold label was found in association with the fibrillar material (arrowheads). Bar equals 0.5 μm. The indistinct spaces between the fibrillar clumps can be confirmed to contain glycogen (asterisk) by tannic acid staining (insert). Bar equals 0.1 μm. (**G**) Higher power of hepatic cytoplasm. Note the gold particle (arrows) labeling adjacent to the RER but not in direct association with any of the numerous ribosomes. Bar equals 0.1 μm.

Laforin has a greater affinity to starch than to glycogen

As previously mentioned, polyglucosans are highly similar to starch. Both are irregularly branched glucose polysaccharides and they differ from glycogen in their lack of a symmetric branching pattern. Laforin was previously shown to be capable of binding to glycogen (15). In the present study, myc–laforin preferentially binds polyglucosan fibrils over glycogen *in vivo* (Fig. 6D–F). To confirm this observation *in vitro* independent of transgenic conditions and cellular factors, we incubated recombinant glutathione *S*-transferase (GST)–laforin with equal concentrations of starch and glycogen, centrifuged the starch and glycogen pellets and analyzed pellets and supernatants by western blotting. The amount of GST–laforin bound to starch was manifold greater than that bound to glycogen (Fig. 7C), indicating a higher affinity of laforin to starch than to glycogen.

EPM2AIP1 localizes to polyglucosans *in vivo*

EPM2AIP1 is the first laforin interacting protein identified. In tissue culture transfection experiments it colocalizes with laforin at the ER (23). Here, we confirm its localization in the vicinity of ER by immunogold electron microscopy (data not shown) and show that like laforin it strongly concentrates on the LB (Fig. 7D and E).

DISCUSSION

LBs indicate the existence of an unknown biochemical pathway, related to glycogen metabolism, defects of which result in starch-like cellular accumulations. The discovery of LD-causing genes has led to the identification of five components of this pathway. These are the laforin DSP (9), the malin ubiquitin E3 ligase (12) and three laforin interacting proteins: EPM2AIP1 (23), HIRIP5 (24) and R5 (25). EPM2AIP1 and HIRIP5 are of yet unknown function, but R5 is a well-studied protein critical to glycogen metabolism. It functions to transport and stabilize glycogen synthase (GS) onto the glycogen particle (26). Coordinated activity between GS and glycogen branching enzyme (BE) then follows. GS elongates glycogen strands, and BE moves these to appropriate branch points to maintain the spherical growth of glycogen and prevent the formation, by GS, of long chains with irregular branching (polyglucosans) (2).

We previously noted that the amino acid sequence of laforin's predicted carbohydrate-binding domain is more similar to starch-binding prokaryote and lower eukaryote enzymes than to mammalian glycogen-binding proteins (such as R5 and GS) (14). In the mice used in this study we show that laforin binds polyglucosans, and that it binds polyglucosans (and starch) preferentially over glycogen. These observations are critical, as they indicate, for the first time, that one of laforin's roles likely begins after the appearance of polyglucosans. We propose that laforin is involved in the quality control of glycogen synthesis. In the simplest explanation, laforin recognizes polyglucosan structures that appear during the course of glycogen synthesis, and it initiates, through its phosphatase domain, mechanisms to counter their continued formation or to promote their elimination. Laforin could also physically interfere with GS activity. Its binding to R5 has been shown to occupy this protein's GS and glycogen-binding regions (25), and would therefore disperse the R5–GS–glycogen complex necessary for further glycogen strand extension.

LBs form in most tissues. In neurons, they compartmentalize in the perikaryon and dendrites, and do not occur in axons (5), an observation replicated in the present model. Accumulation of LBs in sufficient numbers of dendrites by teenage is likely an important cause of the onset and then progression of the epilepsy (2). The comparatively few affected dendrites in the mice in this study may explain the absence of epilepsy in these animals even at 20 months. It appears that the level of laforin's phosphatase substrate is relatively high in comparison with the combined amounts of mutant and wild-type laforin as a 100-fold overexpression of the transgene still resulted in an incomplete phenotype.

Here, we show for the first time that laforin localizes in neuronal dendrites and perikarya, and is excluded from axons, in the same way as LBs (the myc tag is highly unlikely to have confounded this result, as to our knowledge such an effect has not been seen with any other myc-tagged protein). What mediates laforin's dendritic compartmentalization, and is there any glycogen metabolism function that segregates in a similar manner? Glucose 6-phosphatase (G6Pase) is highly enriched in dendritic ER (27), and absent from axonal ER (28). It shunts glucose 6-phosphate (G6P) into the ER, away from GS. G6P is both the substrate and the allosteric activator of GS, and decreases in its concentration have the most potent known effect in the downregulation of GS activity (29). It would be important to determine whether the laforin pathway intersects with the G6Pase complex.

A second feature of dendrites that might underlie laforin's targeting to that compartment is that dendrites possess ribosomes, and axons do not (30) [laforin was shown in tissue culture experiments to reside on ER-associated ribosomes (10)]. We were unable to confirm a laforin-ribosomal association in the mice used in this study. As seen by electron microscopy, laforin did localize near the rough ER in all tissues examined but not on ribosomes. It is possible that either the myc epitope or the cysteine to serine change in the phosphatase domain of the transgene product affected its association with ribosomes. We consider this unlikely, because myc tagging was used in the original tissue culture studies (10), and the cysteine to serine phosphatase change has been shown in many phosphatases studied to strengthen, not weaken, substrate binding, and also not affect protein conformation (31,32). Nonetheless, work is in progress to resolve this point, as it is important to determine whether a laforin substrate exists on rough ER ribosomes, with which laforin's phosphatase domain interacts. In tissue culture experiments, the malin E3 ubiquitin ligase, defects of which also cause LD (12), localizes at the ER. Whether it is on ER ribosomes has not yet been studied, but interaction with laforin in cell culture experiments has been obtained (unpublished data).

Whether malin localizes, with laforin, on LBs or in dendrites could not be determined in the present mice due to the lack of a specific antibody. LBs have been shown to be ubiquitinated (13). It is possible that malin ubiquitinates LBs under the influence of laforin. Alternatively, malin may

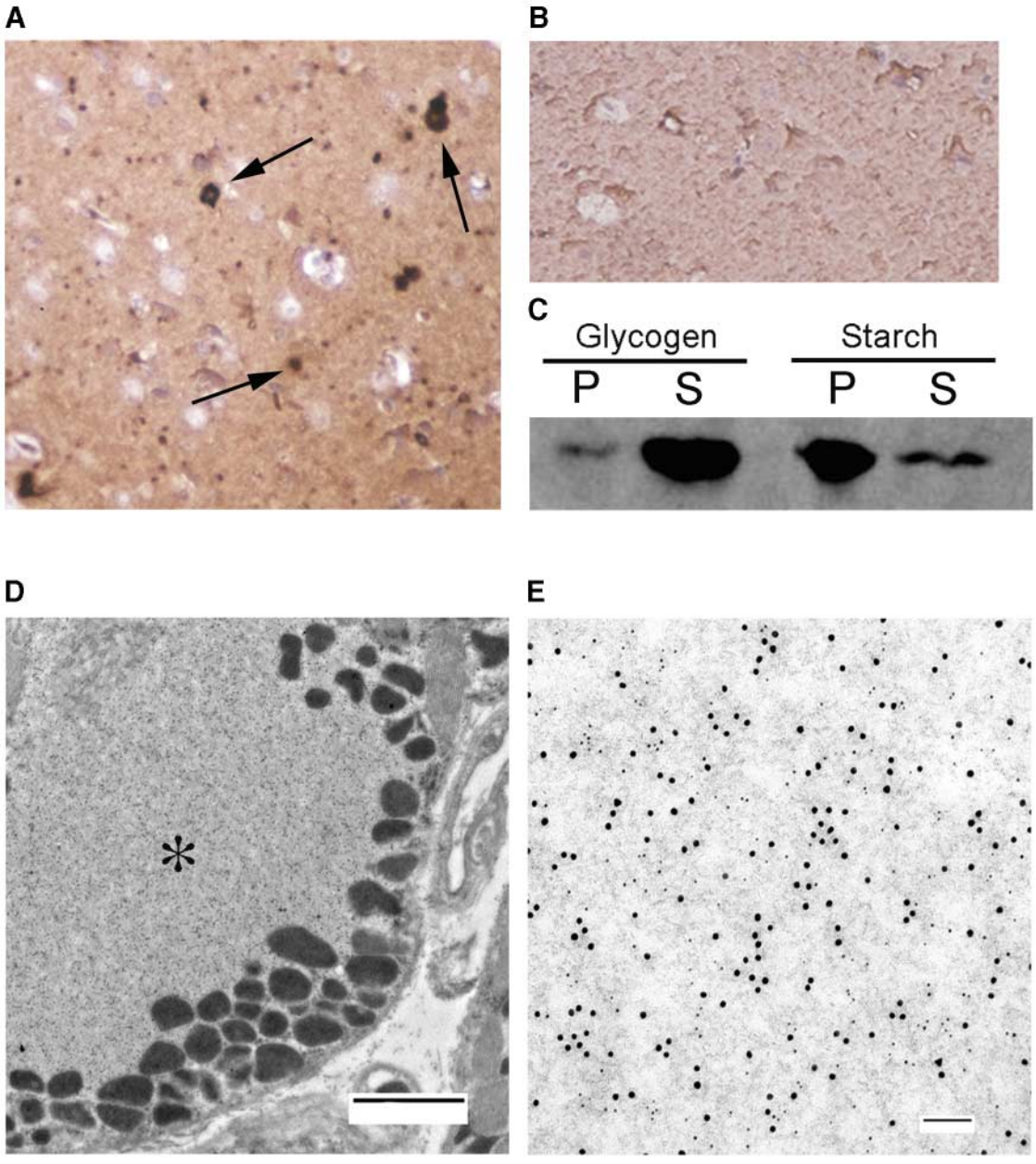

Figure 7. (**A**) R60 (anti-laforin) immunoperoxidase stained section from an LD patient with *EPM2B* mutations [homozygous 98T > C, F33S (12)]. Note the intense labeling of the LBs (arrows). Picture width is 0.75 mm. (**B**) Immunostained section from the same biopsy except that the primary antibody has been omitted. (**C**) Human laforin has a greater affinity to starch than to glycogen. Equal concentrations of glycogen and starch incubated for 1 h with recombinant human GST–laforin and pelleted by ultracentrifugation. GST–Laforin in glycogen and starch supernatant (S) and pellet (P) visualized by western blot using anti-GST antibody. (**D**) Low power electron micrograph of a double-labeled (anti-myc/anti-EPM2AIP1) LB in an affected mouse. Note how the visible label is confined to the LBs (asterisk). Bar equals 2 μm. (**E**) Higher power of (D); note that both the small particles (myc) and the larger particles (EMP2AIP1) are on the polyglucosan fibrils. Bar equals 100 nm.

ubiquitinate enzymes of glycogen synthesis (e.g. GS) and direct them to ubiquitin-mediated degradation. The roles of EPM2AIP1 and HIRIP5, the remaining two known laforin interacting proteins, in LD await to be studied. As an initial step, we show in this work that EPM2AIP1 localizes, with laforin, on the polyglucosan fibrils.

Findings in muscle of the animal model described in this paper include the characteristic storage abnormality. They also include the observation that laforin and LBs localize at the NMJ synapse, specifically at its post-synaptic side, as in brain. This observation is relevant to research in the epilepsy of LD, which, as mentioned, is likely due to diffuse central nervous system (CNS) synaptic dysfunction. The NMJ is more readily amenable to physiological analysis than CNS synapses and can now be used in studies of synaptic function in LD.

In conclusion, a transgenic mouse model of LD has been generated in which polyglucosans form in neurons, hepatocytes and myocytes. Laforin's localization near the ER is confirmed, but its association with the ribosome complex is not. Its presence in dendrites is demonstrated, highlighting the importance of the post-synaptic compartment in LD. For the first time, a direct, *in vivo* and preferential association is shown between the disease-defining polyglucosans and the disease protein laforin. Existence of a cellular pathway, involving laforin and its interacting proteins, that monitors and then arrests the formation of starch-like polyglucosans is suggested and awaits further unveiling.

MATERIALS AND METHODS

Generation of mice expressing a dominant-negative myc–laforin transgene

The eukaryotic expression vector, pCAGGS, was used to deliver the laforin-encoding transgene. This vector consists of the chicken β-actin promoter, CMV-EI enhancer and rabbit β-globin poly(A) signal (22). The transgene was constructed by ligation of the myc–EPM2A cDNA sequence containing a serine substitution of the cysteine residue at amino acid position 266 into the *Eco* RI sites in the expression vector pCAGGS (Fig. 1A). Linear DNA was obtained by double digestion using *Sal*I and *Bsr* BRI. Purification of the DNA by Elutip minicolumns was followed by microinjection into wild-type C57B6/SJL zygote pronuclei that were subsequently transferred into six CD1 pseudopregnant females. Seventy-six offsprings were born and at 14 days tail-blood DNA was isolated by incubation at 55°C overnight in 0.1 M NaCl, 0.1 M EDTA, 0.05 M Tris pH 8.0, 1% SDS and 0.4 mg proteinase K. Saturated salt was added at 30% (v/v) followed by centrifugation. The DNA in the supernatant was precipitated and washed using ethanol.

Integration of the transgene into genomes of the founder mice was analyzed by Southern blot and PCR. The probe used for the former was generated by a *Pst* I digestion of the pCAGGS expression construct containing the dominant-negative myc–EPM2A cDNA. This resulted in a transgene-specific 1.4 kb fragment that positively identified founders containing the myc–laforin transgene (Fig. 1B). This was confirmed by PCR of a 600 bp sequence unique to the transgene (Fig. 1C). Founder transgenic mice were crossed with wild-type 129SvJ mice to produce F1 and F2 offspring for expression and phenotypic analysis.

Real-time quantitative PCR

To compare the quantity of the endogenous and transgenic *EPM2A* transcripts in the same mouse brain tissue, we developed transcript-specific real-time quantitative PCR assays using the SYBR Green detection method (PE Applied Biosystems, ABI PRISM 7900 Sequence Detection System). Specific primers (25 nM) were designed to distinguish endogenous *EPM2A* mRNA [5′-ATGGACACACGGTGTATGTC-3′ (forward) and 5′-AGAAAAGTCTTGTTGTGCTTGA-3′ (reverse)] from the transgenic myc-containing transcript [5′- GTTCGGCTTCTGG CGTGT-3′ (forward) and 5′-GCTTTTGTTCCATGGTTCTG A-3′ (reverse)]. PCR conditions were: 2 min at 50°C, 10 min at 95°C and 40 cycles of 15 s at 95°C, 60 s at 60°C. The PCR reactions were performed in separate tubes and absolute quantitation of the endogenous and transgenic EPM2A transcripts was obtained from mouse brain cDNA. Results were analyzed using the standard curve method according to the manufacturer's instructions (PE Applied Biosystems, ABI PRISM 7900 Sequence Detection System). The standard curve was developed using dilutions of the transcript-specific purified PCR products.

Expression analysis

Brain, liver, skeletal muscle and heart were obtained from F1 mice of founder lines and analyzed for expression of myc–laforin using western blotting. Tissues were homogenized using a rotor-state homogenizer in RIPA buffer [0.1% SDS, 1% deoxycholate, 1% Triton-X, 10 mM Tris–HCl, 15 mM NaCl, 5 mM EDTA, 1% mammalian protease inhibitor cocktail (Sigma-Aldrich, St Louis, MO, USA)]. Insoluble material was removed by centrifuging at 12 000*g* for 10 min at 4°C and the total lysate protein concentrations were determined using the Bio-Rad Protein Assay (Bio-Rad Laboratories, Hercules, CA, USA). An aliquot of 100 μg of total protein lysate from the four tissues was resolved on a 12% SDS polyacrylamide gel for each of the 10 founder lines. The gel was electrotransferred to a nitrocelluose membrane (Bio-Rad Laboratories), which was blocked in 5% milk. A mouse monoclonal antibody to the human c-myc protein (Santa Cruz Biotechnology, Santa Cruz, CA, USA) was used at a concentration of 1 : 1000 in 5% milk. Bound antibodies were detected using a goat anti-mouse secondary antibody and an enhanced chemiluminescence (ECL) detection system (Amersham Biosciences, Piscataway, NJ, USA).

Surgery and electrocorticogram recordings

Surgical implantation of electrodes was performed under pentobarbital anesthesia (35 mg/kg). Surgeries consisted of two frontal and two parietal monopolar electrodes that were placed 1 mm deep, 2.20 mm anterior to bregma and 3 mm lateral from midline (33). All coordinates were measured in millimeters with skull surface flat and bregma 0.0 (34). After surgery, all animals were returned to the animal facility for 4 days of recovery. Each animal was placed in individual warm Plexiglas chambers for a 20 min adaptation period prior to electrocortico gram (ECoG) recordings in order to minimize movement artifact. ECoG recordings were made on paper using a Grass Polysomnograph machine (33,35). All baseline recordings were performed from 1000 to 1400 h to minimize circadian variations.

Light microscopy and immunohistochemistry

Mice were anesthetized by intraperitoneal injection of pentobarbital and perfused via the heart with a solution of 4% paraformaldehyde and 0.1% glutaraldehyde in 0.1 M phosphate buffer (pH 7.2). Brains were removed and cut in the sagittal plane. Half the brain was formalin-fixed overnight, along with portions of skeletal muscle, heart and liver, paraffin-embedded, sectioned and stained using standard histological

technique including diastase (amylase)-digested periodic acid-Schiff (PASD) staining for the specific detection of polyglucosans. Immunohistochemistry was performed on microwave antigen retrieved paraffin sections using an antibody against c-myc at a 1 : 400 dilution. Patient biopsy materials were treated in the same way except that it was incubated with a polyclonal antibody against endogenous laforin (R60) at a dilution of 1 : 10. Immunodetection was performed using a mouse on mouse ABC detection system (myc) or a rabbit on rabbit ABC detection system (R60) (Vector Laboratory, Birmingham, CA, USA).

Transmission and immunogold electron microscopy

Tissues for routine electron microscopy were transferred to universal fixative, minced into 1 mm^3 pieces and fixed for an additional 4 h. Following a thorough rinse in phosphate buffer, tissues were postfixed in 2% OsO_4, dehydrated in acetone and embedded in epon araldite. Sections were then cut and mounted in copper grids, stained in uranyl acetate and lead citrate and then examined and photographed in the transmission electron microscope (TEM).

Tissues for immunogold labeling were again minced into 1 mm^3 pieces and fixed for an additional 4 h in the perfusion fluid. Following several rinses in phosphate buffer, they were infused with 2.3 M sucrose, frozen in liquid nitrogen and freeze-substituted at −85°C in methanol containing 2% uranyl acetate. The specimens were progressively warmed to −20°C where they were infiltrated with Lowicryl HM20 resin (SPI supplies, Westchester, PA, USA) overnight and then polymerized under a UV lamp. Ultrathin sections were prepared and mounted on formvar coated nickel grids. Grids were blocked with phosphate-buffered saline (PBS) containing 0.5% bovine serum albumin (BSA), incubated in the myc antibody at a dilution of 1 : 10 for 1 h, rinsed in PBS/BSA, incubated in goat anti-murine IgG 10 nM gold complexes (Amersham, Oakville, Ontario, Canada) for an additional hour, and washed in PBS followed by distilled water. Procedures for the double labeling experiments were identical to the single labeling experiments except that following blocking the myc labeling was preceded by an overnight incubation at 4°C with a polyclonal antibody against EMP2AIP1. Following several rinses in PBS/BSA the grids were incubated with goat anti-rabbit IgG 5 nM complexes (Amersham) for 1 h. Specimens were again rinsed thoroughly with PBS/BSA prior to labeling with the myc antibody. Samples were stained with uranyl acetate and lead citrate, and then examined and photographed in the TEM. Some of the liver specimens were stained for 30 s in 1% tannic acid following immunogold staining. These samples were also stained with uranyl acetate and lead citrate.

Co-sedimentation with glycogen and starch

GST–laforin fusion protein (11) was expressed in *Escherichia coli* BL21 (DE3 LysS) cells (Stratagene) and purified by affinity chromatography using the BugBuster GST Bind Purification Kit according to the manufacturer's instructions (Novagen). For binding assays, 20 μg of purified recombinant protein was incubated in 100 μl of 50 mM Tris–HCl, pH 7.5, 150 mM NaCl and 0.1% 2-mercaptoethanol containing 2 mg of bovine liver glycogen (Sigma) or soluble starch from potatoes (Sigma) for 1 h at 4°C. Starch was solubilized in binding buffer by heating and shaking at 90°C for 5 min. After the binding, samples were ultracentrifuged at 100 000*g* for 90 min, and the supernatant and the pellet fractions were collected and subjected to western blot analysis using anti-GST antibodies (Santa Cruz Biotechnology).

ACKNOWLEDGEMENTS

We would like to thank Dr O. Carter Snead, III for his support and Ms Aina Tilups for her outstanding technical help in the immunogold electron microscopy preparations. This work is funded by the Hospital for Sick Children Foundation and the Canadian Institutes of Health Research (CIHR). S.W.S. is an investigator of CIHR and an international scholar of the Howard Hughes Medical Institutes. H.L. is supported by the Sigrid Juselius Foundation, Finland.

REFERENCES

1. Lafora, G.R. and Gluck, B. (1911) Beitrag zur histopathologie der myoklonischen epilepsie. *Z. Ges. Neurol. Psychiat.*, **6**, 1–14.
2. Minassian, B.A. (2002) Progressive myoclonus epilepsy with polyglucosan bodies: Lafora disease. *Adv. Neurol.*, **89**, 199–210.
3. Sakai, M., Austin, J., Witmer, F. and Trueb, L. (1970) Studies in myoclonus epilepsy (Lafora body form). II. Polyglucosans in the systemic deposits of myoclonus epilepsy and in corpora amylacea. *Neurology*, **20**, 160–176.
4. Gambetti, P., Di Mauro, S., Hirt, L. and Blume, R.P. (1971) Myoclonic epilepsy with Lafora bodies. Some ultrastructural, histochemical, and biochemical aspects. *Arch. Neurol.*, **25**, 483–493.
5. Cavanagh, J.B. (1999) Corpora-amylacea and the family of polyglucosan diseases. *Brain Res. Brain Res. Rev.*, **29**, 265–295.
6. Van Heycop ten Ham, M. (1974) Lafora disease, a form of progressive myoclonus epilepsy. *Handbook of Clinical Neurology*, **15**, 382–422.
7. Collins, G.H., Cowden, R.R. and Nevis, A.H. (1968) Myoclonus epilepsy with Lafora bodies. An ultrastructural and cytochemical study. *Arch. Pathol.*, **86**, 239–254.
8. Toga, M., Dubois, D. and Hassoun, J. (1968) Ultrastructure of Lafora bodies. *Acta Neuropathol. (Berl.)*, **10**, 132–142.
9. Minassian, B.A., Lee, J.R., Herbrick, J.A., Huizenga, J., Soder, S., Mungall, A.J., Dunham, I., Gardner, R., Fong, C.Y., Carpenter, S. *et al.* (1998) Mutations in a gene encoding a novel protein tyrosine phosphatase cause progressive myoclonus epilepsy. *Nat. Genet.*, **20**, 171–174.
10. Ganesh, S., Agarwala, K.L., Ueda, K., Akagi, T., Shoda, K., Usui, T., Hashikawa, T., Osada, H., Delgado-Escueta, A.V. and Yamakawa, K. (2000) Laforin, defective in the progressive myoclonus epilepsy of Lafora type, is a dual-specificity phosphatase associated with polyribosomes. *Hum. Mol. Genet.*, **9**, 2251–2261.
11. Minassian, B.A., Andrade, D.M., Ianzano, L., Young, E.J., Chan, E., Ackerley, C.A. and Scherer, S.W. (2001) Laforin is a cell membrane and endoplasmic reticulum-associated protein tyrosine phosphatase. *Ann. Neurol.*, **49**, 271–275.
12. Chan, E.M., Young, E.J., Ianzano, L., Munteanu, I., Zhao, X., Christopoulos, C.C., Avanzini, G., Elia, M., Ackerley, C.A., Jovic, N.J. *et al.* (2003) Mutations in NHLRC1 cause progressive myoclonus epilepsy. *Nat. Genet.*, **35**, 125–127.
13. Ganesh, S., Delgado-Escueta, A.V., Sakamoto, T., Avila, M.R., Machado-Salas, J., Hoshii, Y., Akagi, T., Gomi, H., Suzuki, T., Amano, K. *et al.* (2002) Targeted disruption of the *Epm2a* gene causes formation of Lafora inclusion bodies, neurodegeneration, ataxia, myoclonus epilepsy and impaired behavioral response in mice. *Hum. Mol. Genet.*, **11**, 1251–1262.
14. Minassian, B.A., Ianzano, L., Meloche, M., Andermann, E., Rouleau, G.A., Delgado-Escueta, A.V. and Scherer, S.W. (2000) Mutation spectrum and predicted function of laforin in Lafora's progressive myoclonus epilepsy. *Neurology*, **55**, 341–346.

15. Wang, J., Stuckey, J.A., Wishart, M.J. and Dixon, J.E. (2002) A unique carbohydrate binding domain targets the Lafora disease phosphatase to glycogen. *J. Biol. Chem.*, **277**, 2377–2380.
16. Carpenter, S., Karpati, G., Andermann, F., Jacob, J.C. and Andermann, E. (1974) Lafora's disease: peroxisomal storage in skeletal muscle. *Neurology*, **24**, 531–538.
17. Nishimura, R.N., Ishak, K.G., Reddick, R., Porter, R., James, S. and Barranger, J.A. (1980) Lafora disease: diagnosis by liver biopsy. *Ann. Neurol.*, **8**, 409–415.
18. Baumann, R.J., Kocoshis, S.A. and Wilson, D. (1983) Lafora disease: liver histopathology in presymptomatic children. *Ann. Neurol.*, **14**, 86–89.
19. Zhang, J., Somani, A.K., Yuen, D., Yang, Y., Love, P.E. and Siminovitch, K.A. (1999) Involvement of the SHP-1 tyrosine phosphatase in regulation of T cell selection. *J. Immunol.*, **163**, 3012–3021.
20. Maegawa, H., Hasegawa, M., Sugai, S., Obata, T., Ugi, S., Morino, K., Egawa, K., Fujita, T., Sakamoto, T., Nishio, Y. *et al.* (1999) Expression of a dominant negative SHP-2 in transgenic mice induces insulin resistance. *J. Biol. Chem.*, **274**, 30236–30243.
21. Aoki, Y., Huang, Z., Thomas, S.S., Bhide, P.G., Huang, I., Moskowitz, M.A. and Reeves, S.A. (2000) Increased susceptibility to ischemia-induced brain damage in transgenic mice overexpressing a dominant negative form of SHP2. *FASEB J.*, **14**, 1965–1973.
22. Miyazaki, J., Takaki, S., Araki, K., Tashiro, F., Tominaga, A., Takatsu, K. and Yamamura, K. (1989) Expression vector system based on the chicken beta-actin promoter directs efficient production of interleukin-5. *Gene*, **79**, 269–277.
23. Ianzano, L., Zhao, X.C., Minassian, B.A. and Scherer, S.W. (2003) Identification of a novel protein interacting with laforin, the EPM2a progressive myoclonus epilepsy gene product. *Genomics*, **81**, 579–587.
24. Ganesh, S., Tsurutani, N., Suzuki, T., Ueda, K., Agarwala, K.L., Osada, H., Delgado-Escueta, A.V. and Yamakawa, K. (2003) The Lafora disease gene product laforin interacts with HIRIP5, a phylogenetically conserved protein containing a NifU-like domain. *Hum. Mol. Genet.*, **12**, 2359–2368.
25. Fernandez-Sanchez, M.E., Criado-Garcia, O., Heath, K.E., Garcia-Fojeda, B., Medrano-Fernandez, I., Gomez-Garre, P., Sanz, P., Serratosa, J.M. and Rodriguez De Cordoba, S. (2003) Laforin, the dual-phosphatase responsible for Lafora disease, interacts with R5 (PTG), a regulatory subunit of protein phosphatase-1 that enhances glycogen accumulation. *Hum. Mol. Genet.*, **12**, 3161–3171.
26. Fong, N.M., Jensen, T.C., Shah, A.S., Parekh, N.N., Saltiel, A.R. and Brady, M.J. (2000) Identification of binding sites on protein targeting to glycogen for enzymes of glycogen metabolism. *J. Biol. Chem.*, **275**, 35034–35039.
27. Broadwell, R.D. and Cataldo, A.M. (1983) The neuronal endoplasmic reticulum: its cytochemistry and contribution to the endomembrane system. I. Cell bodies and dendrites. *J. Histochem. Cytochem.*, **31**, 1077–1088.
28. Broadwell, R.D. and Cataldo, A.M. (1984) The neuronal endoplasmic reticulum: its cytochemistry and contribution to the endomembrane system. II. Axons and terminals. *J. Comp. Neurol.*, **230**, 231–248.
29. Villar-Palasi, C. and Guinovart, J.J. (1997) The role of glucose 6-phosphate in the control of glycogen synthase. *FASEB J.*, **11**, 544–558.
30. Steward, O. and Banker, G.A. (1992) Getting the message from the gene to the synapse: sorting and intracellular transport of RNA in neurons. *Trends Neurosci.*, **15**, 180–186.
31. Flint, A.J., Tiganis, T., Barford, D. and Tonks, N.K. (1997) Development of 'substrate-trapping' mutants to identify physiological substrates of protein tyrosine phosphatases. *Proc. Natl Acad. Sci. USA*, **94**, 1680–1685.
32. Sun, H., Charles, C.H., Lau, L.F. and Tonks, N.K. (1993) MKP-1 (3CH134), an immediate early gene product, is a dual specificity phosphatase that dephosphorylates MAP kinase *in vivo*. *Cell*, **75**, 487–493.
33. Snead, O.C., III (1988) gamma-Hydroxybutyrate model of generalized absence seizures: further characterization and comparison with other absence models. *Epilepsia*, **29**, 361–368.
34. Paxinos, G. and Watson, C. (1986) *The Rat Brain in Stereotaxic Coordinates,* 2nd edn. Academic Press, San Diego, CA.
35. Cortez, M.A., McKerlie, C. and Snead, O.C., III (2001) A model of atypical absence seizures: EEG, pharmacology, and developmental characterization. *Neurology*, **56**, 341–349.